



Trans. Nonferrous Met. Soc. China 24(2014) 3524-3533

Transactions of Nonferrous Metals Society of China

www.tnmsc.cn

# Hydrogen storage kinetics of nanocrystalline and amorphous Cu–Nd-added Mg<sub>2</sub>Ni-type alloys

Yang-huan ZHANG<sup>1,2</sup>, Sheng XU<sup>1,2</sup>, Ting-ting ZHAI<sup>2</sup>, Tai YANG<sup>2</sup>, Ze-ming YUAN<sup>2</sup>, Dong-liang ZHAO<sup>2</sup>

- 1. Key Laboratory of Integrated Exploitation of Baiyun Obo Multi-Metal Resources, Inner Mongolia University of Science and Technology, Baotou 014010, China;
- 2. Department of Functional Material Research, Central Iron and Steel Research Institute, Beijing 100081, China

Received 5 November 2013; accepted 11 March 2014

**Abstract:** The  $(Mg_{24}Ni_{10}Cu_2)_{100-x}Nd_x$  (x=0, 5, 10, 15, 20) alloys with nanocrystalline and amorphous structures were prepared by melt spinning technology. The structures of the as-cast and spun alloys were characterized by X-ray diffraction (XRD) and high resolution transmission electron microscopy (HRTEM). The effects of Nd content and spinning rate on the structures and hydrogen storage kinetics of the alloys were investigated. The results show that the as-spun Nd-free alloy displays an entire nanocrystalline structure, whereas the as-spun Nd-added alloys hold nanocrystalline and amorphous structures, suggesting that the addition of Nd facilitates the glass forming of the alloys. Both the Nd-addition and the melt spinning significantly improve the gaseous and electrochemical hydrogen storage kinetics of the alloys. The addition of Nd and melt spinning enhance the diffusion ability of hydrogen atoms in the alloy, but both of them impair the charge-transfer reaction on the surface of the alloy electrode, which makes the high rate discharge ability (HRD) of the alloy electrode first mount up and then go down with the growing Nd content and spinning rate.

Key words: hydrogen storage; Nd-addition; melt spinning; phase structures; kinetics

### 1 Introduction

Mg<sub>2</sub>Ni-type metallic hydrides have been looked upon as one of the most promising hydrogen storage materials applied in hydrogen fuel cell vehicle or negative electrodes in Ni-MH batteries [1] because of their major advantages, such as the theoretical gaseous hydrogen absorption capacity of 3.6% and electrochemical capacity of 1000 mA·h/g for Mg<sub>2</sub>NiH<sub>4</sub> [2]. However, the practical application of the alloys is seriously frustrated by their relatively high H-desorption temperatures, sluggish hydriding/dehydriding kinetics and extremely poor electrochemical cycle stabilities no matter as hydrogen storage materials of on-board use or as the negative electrode materials of Ni-MH battery. In spite of facing huge challenges, the researchers in this field are still full of firm confidence to improve the properties of the alloys and have made breakthrough progress.

It is universally convinced that element substitution

and structure modification are effective methods to ameliorate the overall properties of hydrogen storage alloy. To be specific, the partial substitution of some elements (Cu, Fe, V, Cr, Co, Zr, Ti) for Ni in Mg2Ni alloy decreases the stability of the hydride and accelerates the hydrogen desorption reaction [3], and thus substitution is also very effective in preventing the materials from corroding, so as to improve the cycle stability [4–6]. In addition, the substitution of RE (RE= Y, Ce, La) for Mg considerably improves the hydrogen absorption capacity and kinetics of the Mg2Ni alloy due to the catalytic effect of rare earth elements [7,8]. Furthermore, it was verified that the hydriding and dehydriding kinetics of the Mg and Mg-based alloys are strongly affected by their structures [9]. Especially, the as-milled Mg-Ni based-alloys with nanocrystalline and amorphous structures can react with hydrogen even at room temperature and can electrochemically absorb and desorb a large amount of hydrogen at room temperature [10].

High energy ball-milling (HEBM) has inarguably

been considered to be an quite effective method to fabricate nanocrystalline and amorphous Mg and Mg-based alloys. However, the cycle stabilities of the milled Mg and Mg-based alloys are very poor due to the vanishment of the metastable structures generated by ball milling during the multiple hydrogen absorbing and desorbing cycles [11]. Alternatively, the melt-spinning technique is also a useful method to obtain amorphous and/or nanocrystalline structure in the absence of disadvantages inherent to the BM process. It was ascertained that the Mg-based alloys with nanocrystalline and amorphous structures produced by melt-spinning exhibit excellent hydriding characteristics, similar to the alloys produced by the HEBM [12]. Also, the microstructure created by melt spinning displays much higher stability during the hydrogen absorbing and desorbing cycles compared with the microstructure generated by HEBM [13].

Our published works have reported that the substitution of La for Mg and M (M=Cu, Co, Mn) for Ni improved the gaseous and electrochemical hydrogen storage kinetics of the Mg<sub>2</sub>Ni-type alloys dramatically [14]. However, the substitution of other rare earth elements for Mg has not been investigated. On the basis of previous work, we investigated new approaches to improve the hydrogen storage kinetics of Mg<sub>2</sub>Ni-type alloy. In the present work, the effects of Nd content and spinning rate on the structure and hydrogen storage kinetics of the  $(Mg_{24}Ni_{10}Cu_2)_{100-x}Nd_x$  (x=0–20) electrode alloys were investigated.

## 2 Experimental

The experimental alloys with the chemical composition of  $(Mg_{24}Ni_{10}Cu_2)_{100-x}Nd_x(x=0, 5, 10, 15, 20)$  were prepared using a vacuum induction furnace in a helium atmosphere at a pressure of 0.04 MPa to prevent Mg from volatilizing. In order to facilitate the description, the alloys were denoted with Nd content as Nd<sub>0</sub>, Nd<sub>5</sub>, Nd<sub>10</sub>, Nd<sub>15</sub> and Nd<sub>20</sub>, respectively. A part of the as-cast alloys were re-melted and spun by melt spinning with a rotating copper roller cooled by water. The spinning rates used in the experiment were 10, 20, 30 and 40 m/s, respectively, which were approximately expressed by the linear velocity of the copper roller. In order to compare, the as-cast state is defined as the spinning rate of 0 m/s.

The phase structures of the as-cast and as-spun alloys were determined by XRD (D/max/2400). The diffraction, with the experimental parameters of 160 mA, 40 kV and 10 (°)/min respectively, was performed with Cu  $K_{\alpha 1}$  radiation filtered by graphite. The thin film samples of the as-spun alloys prepared by ion etching

technology were observed by HRTEM (JEM-2100F, operated at 200 kV) and their crystalline states were ascertained by electron diffraction (ED).

The hydrogen absorption and desorption kinetics of the alloys were measured by an automatically controlled Sieverts apparatus. Prior to measuring the hydriding and dehydriding kinetics of the alloys, several hydrogen absorbing and desorbing cycles were performed in order to activate the materials. The hydrogen absorption was conducted at 2 MPa (in fact, this pressure was the initial pressure of hydriding process) and 200 °C, and the hydrogen desorption was at a pressure of 1×10<sup>-4</sup> MPa and 250 °C.

The alloys were pulverized by mechanical milling into fine powder with diameter of 30 µm, and then mixing the alloy powder with carbonyl nickel powder in a mass ratio of 1:4. The mixture was cold pressed under a pressure of 35 MPa into round electrode pellet with 15 mm in diameter whose total mass was 1 g. The electrochemical performance was measured at 30 °C using a tri-electrode open cell consisting of a working electrode (the metal hydride electrode), a sintered Ni(OH)<sub>2</sub>/NiOOH counter electrode as well as a Hg/HgO reference electrode, which were immersed in 6 mol/L KOH electrolyte. The voltage between the negative electrode and the reference one was defined as the discharge voltage. In every cycle, the alloy electrode was first charged with a constant current density after resting for 15 min, and it was discharged at the same current density to cut-off voltage of -500 mV.

To determine the electrochemical kinetics of the alloy electrodes, the electrochemical impedance spectra (EIS) and the Tafel polarization curves of the alloys were measured at 303 K using a electrochemical workstation (PARSTAT 2273). Prior to measuring the impedance and polarization curves, several electrochemical charging and discharging cycles were carried out in order to activate the materials. The fresh electrodes were fully charged and then rested for 2 h up to the stabilization of the open circuit potential. The EIS of the alloy electrodes were measured at 50% depth of discharge (DOD), the frequency range from 10 kHz to 5 mHz, the amplitude of signal potentiostatic or galvanostatic measurements being 5 mV, the number of points per decade of frequencies being 60. The Tafel polarization curves were measured in the potential range of -1.2 to +1.0 V (vs Hg/HgO) with a scan rate of 5 mV/s. For the potentiostatic discharge, the test electrodes in the fully charged state were discharged at 500 mV potential step for 5000 s on the electrochemical workstation (PARSTAT 2273), using the electrochemistry corrosion software (CorrWare).

#### 3 Results and discussion

#### 3.1 Microstructure characteristics

Figure 1 shows the XRD patterns of the as-cast and as-spun  $(Mg_{24}Ni_{10}Cu_2)_{100-x}Nd_x$  (x=0-20) alloys. It is evident that the as-spun Nd<sub>0</sub> alloy exhibits very sharp diffraction peaks, indicating that it holds an entire crystalline structure with a grain size of about 20 nm, which was calculated by Scherrer's equation based on the FWHM values of the major diffraction peak (203) in Fig. 1(a). Differing from Nd<sub>0</sub> alloy, the Nd-added alloys display very broad and flat diffraction peaks, indicating that they are of amorphous structure, and the amorphization degree visibly increases with the Nd content rising, suggesting that the addition of Nd facilitates the glass forming in the Mg<sub>2</sub>Ni-type alloy. Meanwhile, it is also found from Fig. 1(b) that the broad and diffuse diffraction peaks of the as-spun (10 m/s) Nd<sub>20</sub> alloy exhibit amorphous and nanocrystalline structures. With the increase of the spinning rate, the diffraction peaks of the Nd<sub>20</sub> alloy become broader and flatter, implying that the amount of amorphous phase is growing. A similar conclusion is also derived by HRTEM detections, as demonstrated in Fig. 2. Clearly, the as-spun Nd<sub>0</sub> alloy was strongly disordered and nanostructured; meanwhile, some crystal defects such as subgrains and grain boundaries can be seen clearly from the locally amplified morphology, and its ED patterns exhibit sharp multi-haloes, corresponding to a nanocrystalline structure. Nevertheless, the as-spun Nd<sub>20</sub> alloy, although spun at the same spinning rate as the Nd<sub>0</sub> alloy, exhibits a clear feature of the nanocrystalline embedded in the amorphous matrix, and its electron diffraction patterns consisted of broad and dull halos, indicating the existence of amorphous structure, which indicates that the addition of Nd facilitates the glass forming of the Mg<sub>2</sub>Ni alloy. In addition, it is found from Figs. 2(c) and (d) that the as-spun (10 and 30 m/s) Nd<sub>5</sub> alloys display obvious nanocrystalline and amorphous structures. Interestingly, the amount of the amorphous phase visibly grows with the spinning rate rising, suggesting that the glass forming ability of the alloy is closely associated with the spinning rate. The existence of the amorphous phase is also evidenced by DSC analysis, as demonstrated in Fig. 3. Evidently, all the as-spun Nd-added alloys display sharp exothermic DSC peaks in the temperature range from 443.8 to 452 °C, indicating that a crystallization reaction (ordering) of the amorphous nanocrystalline takes place. Furthermore, it is found that the varying of Nd content gives rise to the changing of crystallization temperature, suggesting that

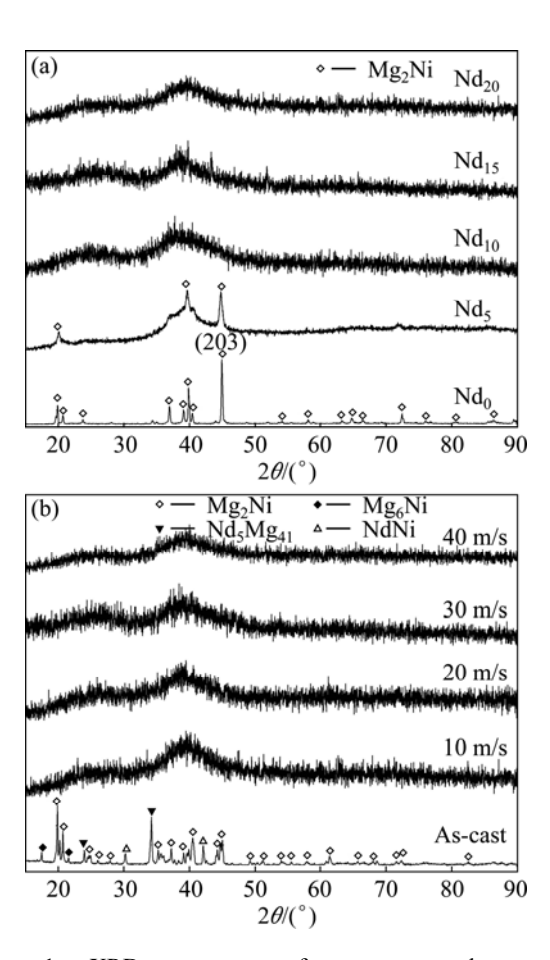


**Fig. 1** XRD patterns of as-cast and as-spun  $(Mg_{24}Ni_{10}Cu_2)_{100-x}Nd_x$  (x=0-20) alloys: (a) As-spun (10 m/s); (b)  $Nd_{20}$  alloy

the stability of the amorphous structure is related to the composition of the alloy.

#### 3.2 Gaseous hydriding and dehydriding kinetics

As is well-known, in addition to the relatively high hydrogen absorption and desorption temperature, the sluggish hydriding and dehydriding kinetics is another issue by which the attempts of putting Mg<sub>2</sub>Ni-type alloy into practice application were severely frustrated. Hence, to examine the influence of Nd-addition and melt spinning on the hydriding and dehydriding kinetics of the alloy is very necessary. Here, the hydriding kinetics of alloy is characterized by its hydrogen absorption saturation ratio ( $R_t^a$ ), a ratio of the hydrogen absorption capacity at a fixed time to the saturated hydrogen absorption capacity of the alloy, which is defined as  $R_t^a = C_t^a / C_{100}^a \times 100\%$ , where  $C_t^a$  and  $C_{100}^a$  are hydrogen absorption capacities at time t and 100 min, respectively. The experimental result indicates that, for all the experimental alloys, the  $C_{100}^{a}$  values are more than 98% of their saturated hydrogen absorption capacities. Therefore, it is reasonable to take the  $C_{100}^{a}$ value as the saturated hydrogen absorption capacity of

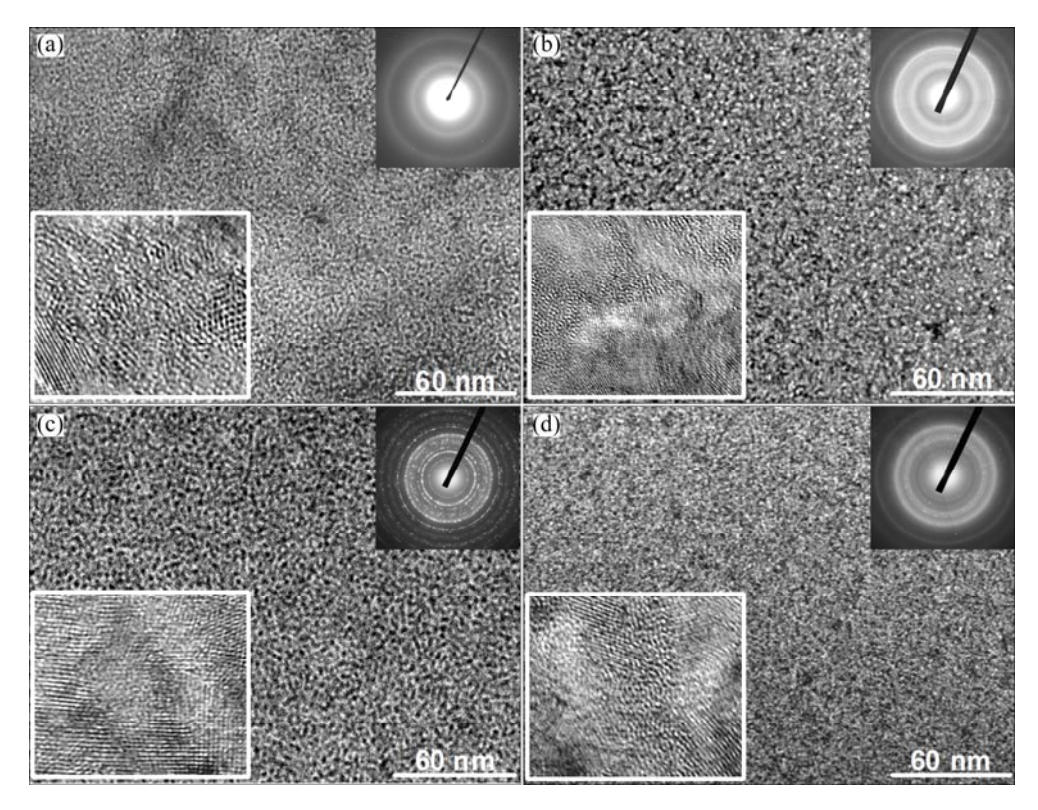


Fig. 2 HRTEM images and ED patterns of as-spun  $(Mg_{24}Ni_{10}Cu_2)_{100-x}Nd_x$  (x=0-20) alloys: (a) As-spun (10 m/s)  $Nd_0$  alloy; (b) As-spun (10 m/s)  $Nd_2$ 0 alloy; (c) As-spun (10 m/s)  $Nd_5$  alloy; (d) As-spun (30 m/s)  $Nd_5$  alloy

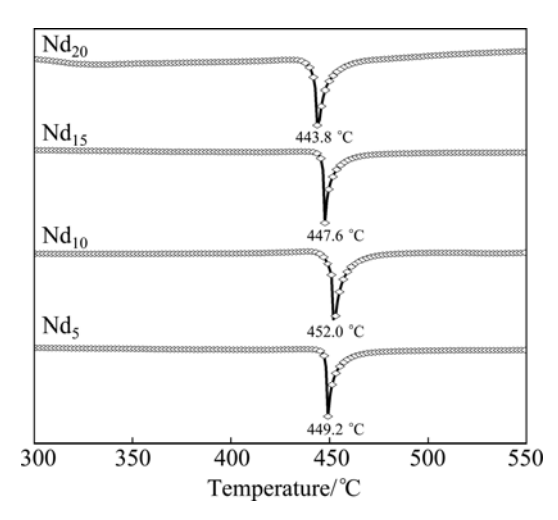
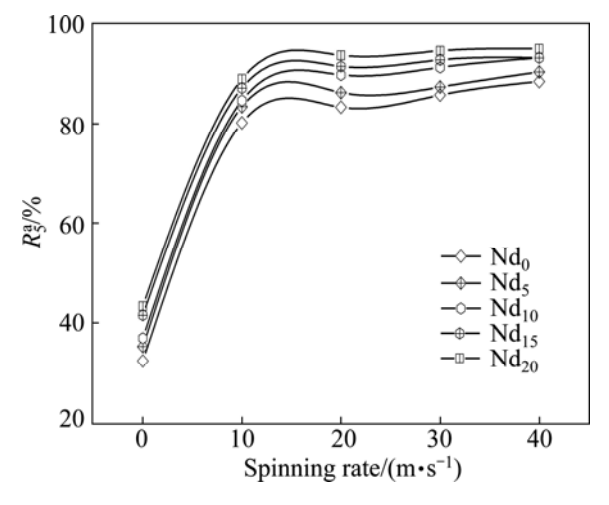


Fig. 3 DSC curves of as-spun (10 m/s) alloys

the alloy. In order to compare, the hydrogen absorption time of 5 min was taken as a criterion. The variations of  $R_5^a$  values of the  $(\mathrm{Mg_{24}Ni_{10}Cu_2})_{100\rightarrow}\mathrm{Nd_x}$  (x=0–20) alloys with the spinning rate are described in Fig. 4, from which it can be found that the melt spinning enhances the hydriding kinetics of the alloys dramatically. In particularly, with the spinning rate rising from 0 to 40 m/s, the  $R_5^a$  value increases from 32.3% to 88.4% for the Nd<sub>0</sub> alloy and from 43.3% to 94.9% for the Nd<sub>20</sub> alloy, respectively. Meanwhile, it can be noticed that whatever the spinning rate is, the  $R_5^a$  values of the



**Fig. 4** Evolution of hydrogen absorption saturation ratio ( $R_5^a$ ) of alloys with varying spinning rate

alloys always increase with the increase of Nd content, indicating that the addition of Nd plays a beneficial role in the hydriding kinetics of the alloy. Noticeably, it can be found that the minimum difference of the  $R_5^a$  values between the as-spun and the as-cast alloys for the fixed Nd content is much larger than the maximum difference of the  $R_5^a$  values generated by the Nd content changing for the fixed spinning rate. So, we powerfully believe that the hydrogen absorption kinetics of the alloy is principally dominated by its structure.

Similarly, the hydrogen desorption kinetics of the alloy is evaluated by hydrogen desorption ratio  $(R_t^d)$ , a ratio of the H-desorbed capacity at a fixed time (t) to the saturated hydrogen absorption capacity of the alloy, which is defined as  $R_t^d = C_t^d / C_{100}^a \times 100\%$ , where  $C_{100}^a$ is the hydrogen absorption capacity at 100 min. and C<sub>1</sub> is the hydrogen desorption capacity at the time t, respectively. For comparison, here, we take hydrogen absorption time of 10 min as the standard. Thus, the relationship between the  $R_{10}^{\rm d}$  (t=10 min) values of the  $({\rm Mg_{24}Ni_{10}Cu_2})_{100-x}{\rm Nd_x}$  (x=0-20) alloys with the spinning rate can be established easily, as illustrated in Fig. 5. Evidently, the melt spinning makes a positive contribution to the dehydriding kinetics of the alloys. More specifically, enhancing the spinning rate from 0 to 40 m/s gives rise to an augment of the  $R_{10}^{\rm d}$  value from 8.2% to 38.9% for the  $Nd_0$  alloy and from 36.1% to 58.2% for the Nd<sub>20</sub> alloy, respectively. Furthmore, it is noticeable that, whatever the spinning rate is, the Nd-added alloy shows a much larger  $R_{10}^{d}$  value than Nd-free one, suggesting that the addition of Nd facilitates the dehydriding rate of the alloy. It is derived that, with the amount of Nd increasing from 0 to 20%, the  $R_{10}^{d}$ value is enhanced from 8.2% to 36.1% for the as-cast alloy and from 38.9% to 58.2% for the as-spun (40 m/s) one, respectively.

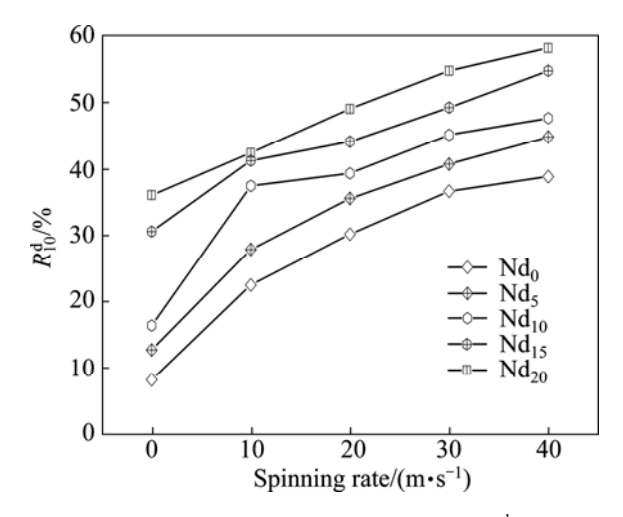


**Fig. 5** Evolution of hydrogen desorption ratio  $(R_{10}^d)$  of alloys with varying spinning rate

Regarding the ameliorated hydriding and dehydriding kinetics by adding Nd and melt spinning, some elucidations can be provided. As is known to all, the hydrogen absorption process of hydrogen storage alloys consists of the following steps: 1) hydrogen molecular dissociation on the surface; 2) hydrogen atoms penetrating from the oxide layer surface into the metal; 3) hydrogen atoms diffusing into the bulk metal; 4) through the hydride already formed. Moreover, the hydrogen absorption rate is predominated by the slowest step. The

positive impact of Nd-addition on the hydriding kinetics is principally ascribed to the enlarged cell volume and the secondary phases created by Nd adding, as evidenced by previous work [14]. CUI and LUO [15] considered that the increase of the lattice constants and cell volume facilitates to decrease the diffusion activation energy of hydrogen atoms, enhancing hydrogen diffusion rate. Also, the secondary phases generated by adding Nd probably engender a catalytic action, weakening the bonding between Mg and H atoms and consequently speeding up the rate of hydrogen diffusion. The hydrogen desorption kinetics improved by adding Nd is ascribed to two reasons. Firstly, the addition of Nd considerably strengthens the glass forming ability of Mg<sub>2</sub>Ni-type alloy because the amorphous structure Mg<sub>2</sub>Ni shows excellent hydrogen desorption capability. Secondly, such substitution decreases the stability of the hydride and makes the desorption reaction easier [3,16]. In respect of the positive contribution engendered by melt spinning to the hydrogen storage kinetics, it is believed to be most likely associated with the changed structure of the alloy by melt spinning. The crystalline material, when melt spun, becomes at least partially disordered and its structure turns into nanocrystalline. generating a lot of new crystallites and grain boundaries (Fig. 2). Hence, some crystal defects such as dislocations, stacking faults and grain boundaries are introduced, as evidenced by our previous work [17], which may prompt the diffusion of hydrogen in materials by providing numerous sites with low diffusion activation energy [18]. Moreover, it was found that the hydriding and dehydriding kinetics of the Mg2Ni-type alloy is very sensitive to its structure. Especially, their hydrogen storage properties are considered to be strongly affected by their nanometer scale structures because of the thermodynamic and kinetic aspects. As reported by KUMARA et al [19], changing the structure from polycrystalline to nanocrystalline renders a decrease of about 100 °C in absorbing/desorbing temperature of the Mg<sub>2</sub>Ni alloy, namely from 300 °C to 200 °C. It is evidenced by ZHAO et al [20] that hydrogen adheres to the surface of the nanocrystalline nickel more strongly polycrystalline nickel, facilitating the dissociation reaction of hydrogen molecular.

#### 3.3 Electrochemical hydrogen storage kinetics

Electrochemical galvanostatic charge/discharge is a more effective and time-saving method for determining the hydrogen storage kinetics than gaseous technique. In general, it is regarded to be extremely important to restrict the sharp degradation of the discharge capacity even at a high charge/discharge current density for the practical application of the hydride electrode in Ni-MH battery. Usually, the electrochemical kinetics of the alloy

is characterized by its HRD, which is defined as HRD=  $C_i/C_{40} \times 100\%$ , where  $C_i$  and  $C_{40}$  are the maximum discharge capacities of the alloy electrode chargeddischarged at the current density i and 40 mA/g respectively. The variations of HRDs of the as-cast and  $(Mg_{24}Ni_{10}Cu_2)_{100-x}Nd_x$ (x=0-20)depending on the discharge current density are presented in Fig. 6. It is noted that the addition of Nd and the melt spinning bring on an evident impact on the HRD of the alloy. In order to demonstrate the influence of the Nd content and the spinning rate on the HRD, the relationships between the HRDs (i=200 mA/g) of the as-spun (10 m/s) alloys and the Nd content and between the HRD of the Nd<sub>20</sub> alloy and the spinning rate are also inserted in Figs. 6(a) and (b), respectively. Obviously, the HRDs of the alloys reach the maximum values with the varying Nd content and the spinning rate. More specifically, with the Nd content increasing from 0 to 20%, the HRD of the as-spun (10 m/s) alloy increases from 69.2% (x=0) to 76.2% (x=10) and then falls to 71.2% (x=20). Likewise, with the spinning rate rising from 0 to 40 m/s, HRD of the Nd<sub>20</sub> alloy mounts up from 52.6% (0 m/s) to 82.1% (20 m/s) and then goes down to 76.1% (40 m/s). Noticeably, it is found that, although a

excess amount of Nd (x>10) or higher spinning rate (>20 m/s) gives rise to an undesired reduction in the HRD, the Nd-added alloys display higher HRD than the Nd-free alloy and the as-spun alloys show larger HRD than the as-cast alloy, which means that the addition of Nd and the melt spinning totally make a positive contribution to the electrochemical kinetics of the alloy.

As a matter of fact, it is believed that the high rate discharge ability of a metal hydride electrode is principally dominated by the charge-transfer rate on the surface of an alloy electrode and the hydrogen diffusion capability in the alloy bulk [21]. Thereby, in order to reveal the mechanism of the improved electrochemical kinetics of the alloy by both the Nd adding and the melt spinning, it is clearly necessary to investigate the effects of the Nd adding and the melt spinning on the diffusion ability of hydrogen atoms and the charge-transfer rate. In the case of hydrogen diffusion ability, it can be quantitatively evaluated by the hydrogen diffusion coefficient, which can be derived by measuring the semilogarithmic curves of anodic current versus working duration of the alloy electrode, as demonstrated in Fig. 7. Based on the model established by ZHENG et al [22], the diffusion coefficient of the hydrogen atoms in the

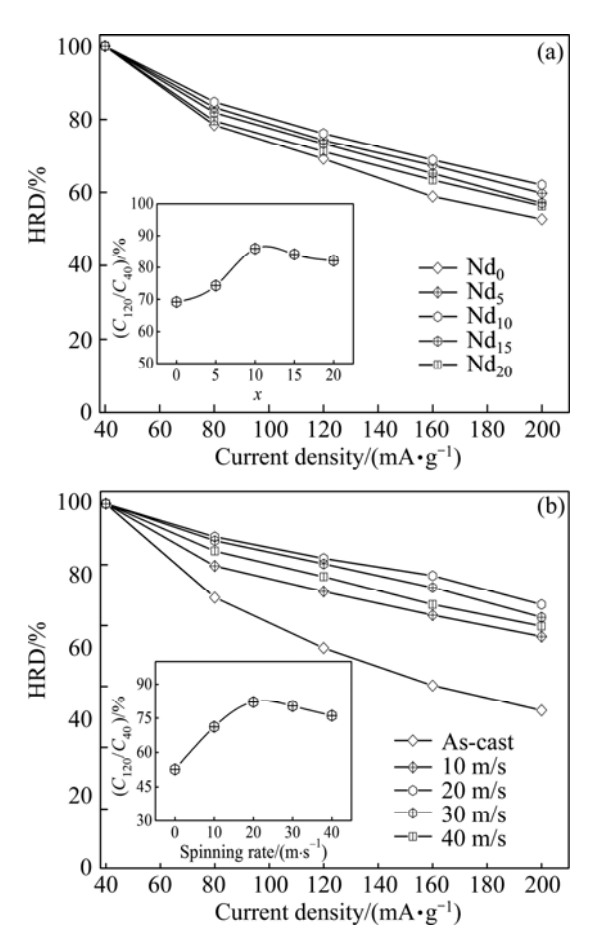


**Fig. 6** Evolution of HRDs of as-cast and as-spun  $(Mg_{24}Ni_{10}Cu_2)_{100-x}Nd_x$  (x=0-20) alloys with varying current density: (a) As-spun (10 m/s); (b)  $Nd_{20}$  alloy

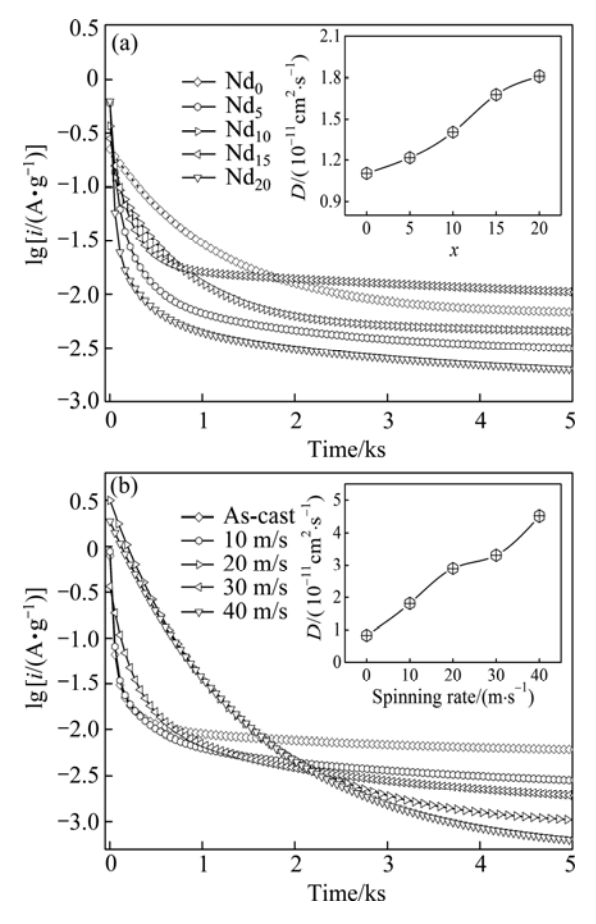


**Fig. 7** Semilogarithmic curves of anodic current vs time responses of as-cast and as-spun  $(Mg_{24}Ni_{10}Cu_2)_{100-x}Nd_x$  (x=0-20) alloys: (a) As-spun (10 m/s); (b)  $Nd_{20}$  alloy

bulk of the alloy could be calculated through the slope of the linear region of the corresponding plots by

$$\lg i = \lg \left( \pm \frac{6FD}{da^2} (C_0 - C_s) \right) - \frac{\pi^2}{2.303} \frac{D}{a^2} t \tag{1}$$

$$D = -\frac{2.303a^2}{\pi^2} \frac{d \lg i}{dt}$$
 (2)

where i is the diffusion current density; D is the hydrogen diffusion coefficient;  $C_0$  is the initial hydrogen concentration in the bulk of the alloy;  $C_s$  is the hydrogen concentration on the surface of the alloy particles; a is the alloy particle radius; d is the density of the hydrogen storage alloy; t is the discharge time. The variations of the D values of the alloys calculated by Eq. (2) with the Nd content and the spinning rate are also inserted in Figs. 7(a) and (b), respectively, which exhibit that the D values of the alloys always grow with the rising of the Nd content and the spinning rate.

Limiting current density  $(i_L)$ , another important electrochemical kinetic characteristic of an alloy electrode, can be obtained by measuring the Tafel polarization curve, as shown in Fig. 8. In all cases,

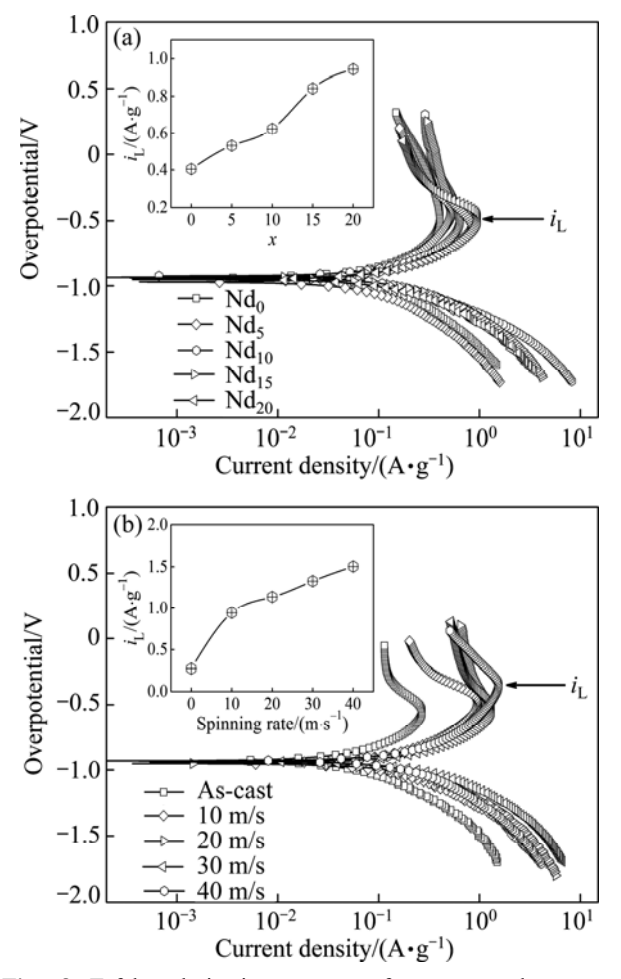


**Fig. 8** Tafel polarization curves of as-cast and as-spun  $(Mg_{24}Ni_{10}Cu_2)_{100-x}Nd_x$  (x=0-20) alloys at 50% DOD: (a) As-spun (10 m/s); (b)  $Nd_{20}$  alloy

an obvious inflection point can be seen in each anodic polarization curve, implying the existence of critical value which is termed as  $i_L$ . It suggests that an oxidation reaction takes place on the surface of the alloy electrode, and the oxidation layer hinders hydrogen atoms from further penetrating [20]. Hence, the  $i_L$  can be viewed as a critical current density of passivation which is basically dominated by the diffusion rate of hydrogen in alloy electrode [23]. The  $i_L$  values of the alloys as functions of the Nd content and the spinning rate are also presented in Figs. 8(a) and (b), respectively. Evidently, the  $i_L$  values of the alloys monotonously increase with the Nd content and the spinning rate growing.

As for the charge-transfer ability, it can be qualitatively evaluated by its EIS, as shown in Fig. 9. Clearly, it can be seen that each EIS spectrum contains two distorted capacitive loops at high and middle frequencies as well as a straight line at low frequencies, which reflects the electrochemical processes very well, as elucidated and modeled by KURIYAMA et al [24]. The smaller semicircle in the high frequency region corresponds to the contact resistance between the alloy powder and the conductive material, and the larger one in the middle frequency region equals the charge-transfer

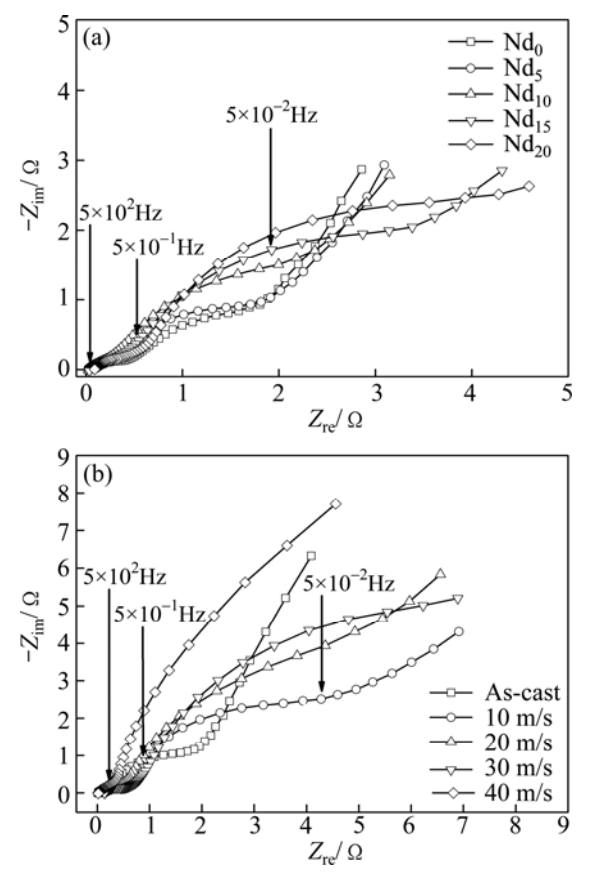


**Fig. 9** Electrochemical impedance spectra (EIS) of as-cast and as-spun  $(Mg_{24}Ni_{10}Cu_2)_{100-x}Nd_x$  (x=0-20) alloys at 50% DOD: (a) As-spun (10 m/s); (b)  $Nd_{20}$  alloy

resistance on the alloy surface while the straight line in low frequency relates to the atomic hydrogen diffusion in the alloy. Apparently, the larger the radius of the semicircle in the middle frequency region is, the higher the charge-transfer resistance of the alloy electrode will be. It can be seen that the radii of the large semicircles of the alloy electrodes in the middle frequency region markedly expand with the Nd content and the spinning rate increasing. Especially, the straight lines on EIS spectrum of the as-spun (>20 m/s) Nd<sub>20</sub> alloy almost disappear, suggesting that both the addition of Nd and the melt spinning impair the charge-transfer ability on the surface of the alloy electrode significantly.

Based on the above-mentioned results, some acceptable elucidations can be offered as reasons why the addition of Nd and the melt spinning result in a notable change of the HRD and electrochemical kinetics of the alloys. The electrochemical hydriding/dehydriding reaction taking place at the hydrogen storage electrode in an alkaline solution during charging and discharging process can be expressed by

$$M + \frac{x}{2}H_2O + \frac{x}{2}e \longleftrightarrow MH_x + \frac{x}{2}OH^-$$
 (3)

where M is the hydrogen storage alloy. The hydrogen atom adhered to the surface of the alloy electrode is suggested to have two possible whereabouts, combining together to form hydrogen molecule or producing metal hydride via diffusion. That is to say, the diffusion rate of hydrogen atom within the surface layer of alloy determines the utilization of charging current, which is just the ratio of the diffusion current to the imposing current. It can be seen from Eq. (3) that when the alloy electrode is charged in KOH solution, it electrolytically makes hydrogen atoms at the alloy-electrolyte interface diffuse into bulk alloy, and then stores them in the metallic lattice in the form of hydride. In the process of discharging, the hydrogen stored in the bulk alloy diffuses toward the surface where it is oxidized. Evidently, the electrochemical hydrogen storage kinetics of the alloy electrode is determined by the chargetransfer rate on the surface of the alloy electrode and the hydrogen diffusion capability in the alloy bulk. From the enhanced diffusion ability of hydrogen atoms and the lowered charge-transfer rate by Nd adding and melt spinning, it can be convinced that both the addition of Nd and the melt spinning play beneficial and harmful roles in the HRD of the alloy simultaneously. It is different actions incurred by Nd adding and melt spinning that make the HRD of the alloy first mount up and then go down with the varying Nd content and the spinning rate.

In terms of the hydrogen diffusion, it is convinced to be dominated by the strength of the metal-hydrogen interaction as well as the structure of the alloy [25]. The addition of transition metals improves the hydriding properties of Mg<sub>2</sub>Ni-type alloy markedly. Transition metals, such as Ni, Co and Cu, act as catalysts to weaken the bond between Mg and H atoms, thus bringing on an increase in hydrogen diffusion ability. Furthermore, the positive impact of the enlarged cell volume by adding elements and the refined grains by melt spinning on hydrogen diffusion has been mentioned before, so here it is needless to say. In the case of the charge-transfer step, KLEPERIS et al [26] considered that it is controlled by both crystallographic and electronic structures. The variation of the alloy compositions on the alloy surface results in an evident impact on the valence electron configurations, which dominates the charge-transfer reaction, namely the hydrogen dissociative reaction [27]. The experimental results indicate that the addition of Nd and the melt spinning bring on a negative impact on the charge-transfer, which is ascribed to the change of the structure originated from the adding Nd and the melt spinning. The increased cell volume by Nd adding and the ultra-refined grains by melt spinning dramatically enhance the anti-pulverization ability of the alloy during electrochemical cycling, which means producing fewer fresh surface of the alloy, so as to impair the charge-transfer ability.

#### 4 Conclusions

- 1) The as-spun Nd-free alloy displays an entire nanocrystalline structure, whereas the as-spun Nd-added alloys obviously show an amorphous structure, which confirms that the addition of Nd facilitates the glass forming of the  $Mg_2Ni$ -alloys.
- 2) Both the Nd adding and the melt spinning make the positive contribution to the gaseous hydrogen storage kinetics of the alloys. As a result, the hydrogen absorption saturation ratio and hydrogen desorption ratio monotonously grow with the rising of the Nd content and the spinning rate.
- 3) Both the addition of Nd and the melt spinning play a beneficial role in the electrochemical kinetics of the alloys. Differing from the gaseous hydrogen storage kinetics, the HRD values of the alloy electrodes first increase and then decline with the varying Nd content and the spinning rate, for which the enhanced diffusion ability of hydrogen atoms and the impaired charge-transfer rate by both Nd adding and melt spinning rate are basically responsible.

#### References

- [1] EBRAHIMI-PURAANI A, KASHANI-BOZORG S F. Nanocrystalline  $Mg_2Ni$ -based powders produced by high-energy ball milling and subsequent annealing [J]. Journal of Alloys and Compounds, 2008, 456(1-2): 211-215.
- [2] SCHLAPBACH L, ZÜTTEL A. Hydrogen-storage materials for mobile applications [J]. Nature, 2001, 414: 353–358.
- [3] ZHANG Yang-huan, ZHAO Dong-liang, LI Bao-wei, QI Yan, GUO Shi-hai, WANG Xin-lin. Hydrogen storage behaviours of nanocrystalline and amorphous Mg<sub>20</sub>Ni<sub>10-x</sub>Co<sub>x</sub> (x=0-4) alloys prepared by melt spinning [J]. Transactions of Nonferrous Metals Society of China, 2010, 20(3): 405–411.
- [4] GOO N H, JEONG W T, LEE K S. Effects of Zr addition on discharge properties of mechanically alloyed Mg2Ni hydrogenstorage alloy electrode [J]. Journal of Power Sources, 2000, 87(1–2): 118–124.
- [5] LIU Bao-zhong, LI An-ming, FAN Yan-ping, HU Meng-juan, ZHANG Bao-qing. Phase structure and electrochemical properties of La<sub>0.7</sub>Ce<sub>0.3</sub>Ni<sub>3.75</sub>Mn<sub>0.35</sub>Al<sub>0.15</sub>Cu<sub>0.75-x</sub>Fe<sub>x</sub> hydrogen storage alloys [J]. Transactions of Nonferrous Metals Society of China, 2012, 22(11): 2730–2735.
- [6] WEI Fan-song, LI Li, XIANG Hong-fu, LI Hui, WEI Fan-na. Phase structure and electrochemical properties of La<sub>1.7+x</sub>Mg<sub>1.3-x</sub>(NiCoMn)<sub>9.3</sub> (x=0-0.4) hydrogen storage alloys [J]. Transactions of Nonferrous Metals Society of China, 2012, 22(8): 1995–1999.
- [7] SPASSOV T, KÖSTER U. Hydrogenation of amorphous and nanocrystalline Mg-based alloys [J]. Journal of Alloys and Compounds, 1999, 287(1–2): 243–250.
- [8] ZHANG Y H, HOU Z H, YANG T, ZHANG G F, LI X, ZHAO D L. Structure and electrochemical hydrogen storage characteristics of La<sub>0.8-x</sub>Pr<sub>x</sub>Mg<sub>0.2</sub>Ni<sub>3.15</sub>Co<sub>0.2</sub>Al<sub>0.1</sub>Si<sub>0.05</sub> (x=0-0.4) electrode alloys [J]. Journal of Central South University of Technology, 2013, 20(5): 1142-1150.
- [9] ZHANG Yang-huan, LÜ Ke, ZHAO Dong-liang, GUO Shi-hai, QI Yan, WANG Xin-lin. Electrochemical hydrogen storage characteristics of nanocrystalline and amorphous Mg<sub>2</sub>Ni-type alloys prepared by melt-spinning [J]. Transactions of Nonferrous Metals Society of China, 2011, 21(3): 502–511.
- [10] SAKINTUNA B, LAMARI-DARKRIM F, HIRSCHER M. Metal hydride materials for solid hydrogen storage: A review [J]. International Journal of Hydrogen Energy, 2007, 32(9): 1121–1140.
- [11] SONG M Y, KWON S N, BAE J S, HONG S H. Hydrogen-storage properties of Mg–23.5Ni– (0 and 5)Cu prepared by melt spinning and crystallization heat treatment [J]. International Journal of Hydrogen Energy, 2008, 33(6): 1711–1718.
- [12] TODOROVA S, SPASSOV T. Mg<sub>6</sub>Ni formation in rapidly quenched amorphous Mg-Ni alloys [J]. Journal of Alloys and Compounds, 2009, 469(1-2): 193-196.
- [13] LIANG G Y, WU D C, LI L, HUANG L J. A discussion on decay of discharge capacity for amorphous Mg–Ni–Nd hydrogen storage alloy [J]. Journal of Power Sources, 2009, 186(2): 528–531.
- [14] ZHANG Y H, LI B W, REN H P, HOU Z H, HU F, WANG X L. Influences of melt spinning on electrochemical hydrogen storage

- performance of nanocrystalline and amorphous Mg<sub>2</sub>Ni-type alloys [J]. Journal of Central South University of Technology, 2011, 18(6): 1825–1832.
- [15] CUI N, LUO J L. Electrochemical study of hydrogen diffusion behavior in Mg<sub>2</sub>Ni-type hydrogen storage alloy electrodes [J]. International Journal of Hydrogen Energy, 1999, 24(1): 37–42.
- [16] ZHANG Y H, QI Y, REN H P, MA Z H, GUO S H, ZHAO D L. Hydriding and dehydriding kinetics of nanocrystalline and amorphous Mg<sub>2</sub>Ni<sub>1-x</sub>Mn<sub>x</sub> (x=0-0.4) alloys prepared by melt spinning [J]. Journal of Central South University of Technology, 2011, 18(4): 985–992
- [17] ZHANG Yang-huan, ZHAO Dong-liang, LI Bao-wei, GUO Shi-hai, QI Yan, WANG Xin-lin. Influence of rapid quenching on hydrogen storage characteristics of nanocrystalline Mg<sub>2</sub>Ni-type alloys [J]. Transactions of Nonferrous Metals Society of China, 2010, 20(8): 1439–1446.
- [18] WU Y, HANA W, ZHOU S X, LOTOTSKY M V, SOLBERG J K, YARTYS V A. Microstructure and hydrogenation behavior of ball-milled and melt-spun Mg-10Ni-2Mm alloys [J]. Journal of Alloys and Compounds, 2008, 466(1-2): 176-181.
- [19] KUMARA L H, VISWANATHAN B, MURTHY S S. Hydrogen absorption by Mg<sub>2</sub>Ni prepared by polyol reduction [J]. Journal of Alloys and Compounds, 2008, 461(1-2): 72-76.
- [20] ZHAO X Y, DING Y, MA L Q, WANG L Y, YANG M, SHEN X D. Electrochemical properties of MmNi<sub>3.8</sub>Co<sub>0.75</sub>Mn<sub>0.4</sub>Al<sub>0.2</sub> hydrogen storage alloy modified with nanocrystalline nickel [J]. International Journal of Hydrogen Energy, 2008, 33(22): 6727–6733.
- [21] RATNAKUMAR B V, WITHAM C, BOWMAN R C Jr, HIGHTOWER A, FULTZ B. Electrochemical studies on LaNi<sub>5-x</sub>Sn<sub>x</sub> metal hydride alloys [J]. Journal of the Electrochemical Society, 1996, 143(8): 2578–2584.
- [22] ZHENG G, POPOV B N, WHITE R E. Electrochemical determination of the diffusion coefficient of hydrogen through a LaNi<sub>4.25</sub>Al<sub>0.75</sub> electrode in alkaline aqueous solution [J]. Journal of the Electrochemical Society, 1995, 142(8): 2695–2698.
- [23] LIU Y F, PAN H G, GAO M X, ZHU Y F, LEI Y Q, WANG Q D. The effect of Mn substitution for Ni on the structural and electrochemical properties of La<sub>0.7</sub>Mg<sub>0.3</sub>Ni<sub>2.55-x</sub>Co<sub>0.45</sub>Mn<sub>x</sub> hydrogen storage electrode alloys [J]. International Journal of Hydrogen Energy, 2004, 29(3): 297–305.
- [24] KURIYAMA N, SAKAI T, MIYAMURA H, UEHARA I, ISHIKAWA H, IWASAKI T. Electrochemical impedance and deterioration behavior of metal hydride electrodes [J]. Journal of Alloys and Compounds, 1993, 202(1–2): 183–197.
- [25] ZHAO X Y, DING Y, YANG M, MA L Q. Effect of surface treatment on electrochemical properties of MmNi<sub>3.8</sub>Co<sub>0.75</sub>Mn<sub>0.4</sub>Al<sub>0.2</sub> hydrogen storage alloy [J]. International Journal of Hydrogen Energy, 2008, 33(1): 81–86.
- [26] KLEPERIS J, WÓJCIK G, CZERWINSKI A, SKOWRONSKI J, KOPCZYK M, BELTOWSKA-BRZEZINSKA M. Electrochemical behavior of metal hydrides [J]. Journal of Solid State Electrochemistry, 2001, 5(4): 229–249.
- [27] NOBUHARA K, KASAI H, DINO W A, NAKANISHI H.  $\rm H_2$  dissociative adsorption on Mg, Ti, Ni, Pd and La surfaces [J]. Surface Science, 2004, 566–568: 703–707.

# 添加 Cu-Nd 的 Mg<sub>2</sub>Ni 型纳米晶和 非晶合金的吸氢动力学性能

张羊换1,2, 许胜1,2, 翟亭亭2, 杨泰2, 袁泽明2, 赵栋梁2

- 1. 内蒙古科技大学 内蒙古自治区白云鄂博矿多金属资源综合利用重点实验室,包头 014010;
  - 2. 钢铁研究总院 功能材料研究所, 北京 100081

摘 要:采用快淬方法制备添加 Cu 及 Nd 元素的具有纳米晶和非晶结构的(Mg24Ni<sub>10</sub>Cu2)<sub>100-x</sub>Nd<sub>x</sub> (x=0,5,10,15,20) 合金。用 X 射线衍射(XRD)和高分辨率投射电镜(HRTEM)分析铸态及快淬态合金的相组成及结构,并研究 Nd 含量和快淬速率对合金相结构及吸氢性能的影响。结果表明,快淬态无 Nd 合金为纳米晶结构,而含 Nd 的快淬态合金则为纳米晶和非晶结构,表明添加 Nd 促进了合金的非晶形成能力。添加 Nd 及快淬处理均显著地促进了合金的气态及电化学动力学性能。添加 Nd 及快淬处理加快了氢原子在合金体内的扩散速率,但是均降低了合金电极表面的电荷传递性能,从而使得合金的高倍率放电性能(HRD)随着 Nd 含量和快淬速率的增加先上升而后下降。关键词: 贮氢;添加 Nd;快淬;相结构;动力学

(Edited by Xiang-qun LI)